Mass Transfer Between Flowing Fluid and Sphere Buried in Packed Bed of Inerts

J. R. F. Guedes de Carvalho, J. M. P. Q. Delgado, and M. A. Alves
Dept. de Engenharia Química, Faculdade de Engenharia da Universidade do Porto, Rua Dr. Roberto Frias, 4200-465 Porto, Portugal

The equations describing fluid flow and mass transfer around a sphere buried in a packed bed are presented, with due consideration given to the processes of transverse and longitudinal dispersion. Numerical solution of the equations was undertaken to obtain point values of the Sherwood number as a function of the Peclet and Schmidt numbers over a wide range of values of the relevant parameters. A correlation is proposed that describes accurately the dependence found numerically between the values of the Sherwood number and the values of Peclet and Schmidt numbers. Experiments on the dissolution of solid spheres (benzoic acid and 2-naphthol) buried in packed beds of sand, through which water was forced, at temperatures in the range 293 K to 373 K, gave values of the Sherwood number that were used to test the theoretical results obtained. Excellent agreement was found between theory and experiment, including the large number of available data for naphthalene–air, and this helps establish the proposed correlation as "general" for mass transfer between a buried sphere and the fluid (liquid or gas) flowing around it. *AIChE J,* 50: 65–74, 2004
Keywords: mass transfer, dispersion, packed bed, active sphere, liquid flow

Introduction

In several situations of practical interest a large solid mass interacts with the liquid flowing around it through the interstices of a packed bed of inerts. Examples are the leaching of buried rocks and the contamination of underground waters by compacted buried waste. The dissolution of a slightly soluble sphere buried in a packed bed of sand, through which water flows, is a useful model for such processes, and it is considered in the present work.

This study may be seen as a natural extension of work made by our team (Coelho and Guedes de Carvalho, 1988b; Guedes de Carvalho and Alves, 1999) on mass transfer around a sphere buried in a packed bed through which gas flows, which is important in the analysis of char combustion in fluidized beds. From a fundamental point of view, working with water has great interest, since it allows a considerable variation in the value of the Schmidt number, Sc. Indeed, whereas Sc is of order 1 for most gas mixtures, it is possible to cover the approximate range $50 < Sc < 1000$ by working with common solutes in water, at temperatures between 290 and 373 K.

In a recent study on transverse dispersion in liquids, Delgado and Guedes de Carvalho (2001) showed that there is a significant dependence between D_T and Sc, in the range $Sc < 550$. Since the rate of mass transfer around a buried sphere exposed to a flowing fluid is strongly determined by D_T (see Guedes de Carvalho and Alves, 1999), it may be expected that this mass transfer will show a significant dependence on Sc.

The only data available on mass transfer between a sphere immersed in a packed bed of inerts and the liquid flowing around it seem to be those of Guedes de Carvalho and Delgado (1999), who worked with water near ambient temperature. Their results showed that the approach of Coelho and Guedes de Carvalho (1988b) could be extended to predict the rates of mass transfer in liquids at high values of the Peclet number, Pe' (based on the diameter of the sphere).

The present work was undertaken in an effort to both widen the range of application of the theoretical analysis and provide experimental data over a substantial range of values of Sc.

Theory

In terms of analysis, we consider the situation of a slightly soluble sphere of diameter d_1 buried in a bed of inert particles

Correspondence concerning this article should be addressed to J. R. F. Guedes de Carvalho at jrguedes@fe.up.pt.

of diameter d (with $d \ll d_1$), packed uniformly (void fraction ϵ) around the sphere. The packed bed is assumed to be "infinite" in extent, and a uniform interstitial velocity of liquid, $\boldsymbol{u}_0$, is imposed at a great distance from the sphere.

Darcy's law, $\boldsymbol{u} = -K\boldsymbol{grad}p$, is assumed to hold, and if it is coupled with the continuity relation for an incompressible fluid, div $\boldsymbol{u} = 0$, Laplace's equation $\nabla^2\phi = 0$ is obtained for the flow potential, $\phi = Kp$, around the sphere.

In terms of spherical coordinates (r, θ), the potential and stream functions are, respectively (see Currie, 1993)

$$\phi = -u_0\left[1 + \frac{1}{2}\left(\frac{R}{r}\right)^3\right] r\cos\theta \tag{1}$$

$$\psi = \frac{u_0}{2}\left[1 - \left(\frac{R}{r}\right)^3\right] r^2\sin^2\theta \tag{2}$$

and the velocity components are

$$u_r = \frac{\partial\phi}{\partial r} = -u_0\cos\theta\left[1 - \left(\frac{R}{r}\right)^3\right] \tag{3}$$

$$u_\theta = \frac{1}{r}\frac{\partial\phi}{\partial\theta} = u_0\sin\theta\left[1 + \frac{1}{2}\left(\frac{R}{r}\right)^3\right]. \tag{4}$$

The analysis of mass transfer is based on a steady-state material balance on the solute crossing the borders of an elementary volume, limited by the potential surfaces ϕ and $\phi + \delta\phi$, and the stream surfaces ψ and $\psi + \delta\psi$. The resulting equation is (see Guedes de Carvalho and Alves, 1999)

$$\frac{\partial c}{\partial\phi} = \frac{\partial}{\partial\phi}\left(D_L\frac{\partial c}{\partial\phi}\right) + \frac{\partial}{\partial\psi}\left(D_T\omega^2\frac{\partial c}{\partial\psi}\right) \tag{5}$$

where ω is the distance to the flow axis, and D_L and D_T are the longitudinal and transverse dispersion coefficients, respectively.

The boundary conditions to be observed in the integration of Eq. 5 are: (1) the solute concentration is equal to the background concentration, c_0, far away from the sphere; (2) the solute concentration is equal to the equilibrium concentration, $c = c^*$, on the surface of the sphere; and (3) the concentration field is symmetric about the flow axis.

The procedure followed in the numerical solution of Eq. 5, with the appropriate boundary conditions, is an improved version of the method described by Guedes de Carvalho and Alves (1999), and it is detailed in Appendix A.

The numerical solution of Eq. 5 gives the concentration field, and from it the instant rate of dissolution of the sphere, n, is obtained by integrating the diffusion/dispersion flux over the surface $r = R$

$$n = -\int_0^\pi \epsilon D_T\left(\frac{\partial c}{\partial r}\right)_{r=R} 2\pi\omega R d\theta \tag{6}$$

This integral may be evaluated numerically for each set of conditions from the discretized concentration field that is obtained through the numerical solution of Eq. 5 (see Appendix A). It is convenient to express the rate of dissolution in terms of the Sherwood number, $Sh' = kd_1/D'_m$, where $k = n/[\pi d_1^2(c^* - c_0)]$ is the mass-transfer coefficient for the sphere. (The effective coefficient of molecular diffusion for the solute is $D'_m = D_m/\tau$, where τ is the tortuosity; in all primed dimensionless groups, D'_m is used instead of D_m).

In the analysis of the results of the numerical computations, it is convenient to consider two separate ranges of $Pe'_p (= u_0 d/D'_m)$.

1. Low Pe'_p (say, $Pe'_p < 0.1$). For very low Pe'_p, dispersion is the direct result of molecular diffusion, with $D_T = D_L = D'_m$, and the numerical solution obtained by Guedes de Carvalho and Alves (1999) applies. Those authors suggest that their results are well approximated (with an error of less than 1% in Sh') by

$$\frac{Sh'}{\epsilon} = \left[4 + \frac{4}{5}(Pe')^{2/3} + \frac{4}{\pi}Pe'\right]^{1/2} \tag{7}$$

where $Pe' = u_0 d_1/D'_m$ is the Peclet number for the sphere.

2. Intermediate to high Pe'_p (say, $Pe'_p > 0.1$). As Pe'_p is increased above 0.1, values of D_T and D_L start to deviate from D'_m, and this has to be taken into account in the integration of Eq. 5. For gas flow, it is generally accepted that good approximate values are given by

$$D_L = D'_m + \frac{ud}{Pe_L(\infty)} \quad \text{or} \quad \frac{D_L}{D'_m} = 1 + \frac{Pe'_p}{Pe_L(\infty)}\frac{u}{u_0} \tag{8}$$

$$D_T = D'_m + \frac{ud}{Pe_T(\infty)} \quad \text{or} \quad \frac{D_T}{D'_m} = 1 + \frac{Pe'_p}{Pe_T(\infty)}\frac{u}{u_0} \tag{9}$$

for the entire range of values of Pe'_p, with $Pe_L(\infty) = 2$ and $Pe_T(\infty) = 12$, for flow through beds of approximately isometric particles (see Wilhelm, 1962; Coelho and Guedes de Carvalho, 1988a).

The numerical solution of Eq. 5, with D_L and D_T given by Eqs. 8 and 9, was worked out by Guedes de Carvalho and Alves (1999), who observed that the values of Sh' obtained from the numerical solution are well represented (within 2% in Sh') by

$$\frac{Sh'}{\epsilon} = \left[4 + \frac{4}{5}(Pe')^{2/3} + \frac{4}{\pi}Pe'\right]^{1/2}\left(1 + \frac{Pe'_p}{9}\right)^{1/2} \tag{10}$$

Now, for liquids, since Eqs. 8 and 9 are still good approximations at low to intermediate values of Pe'_p (say, up to $Pe'_p \approx 1$, for D_L, and up to $Pe'_p \approx 10$, for D_T), Eq. 10 will be adequate, but only for a narrow range of Pe'_p. Beyond that range, more accurate values of D_T and D_L are required, in the numerical solution of Eq. 5.

Values of D_T for liquid flow have been reported recently by Delgado and Guedes de Carvalho (2001) and Guedes de Carvalho and Delgado (2000) in what seems to be the only available study on the influence of Sc on D_T. Their data for the

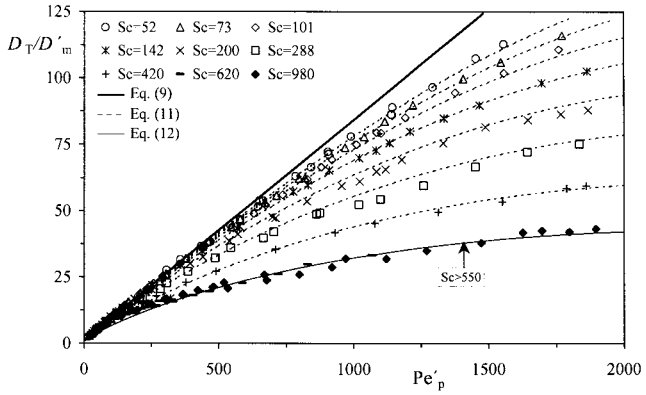

Figure 1. Experimental values of D_T/D'_m for $Pe'_p < 2000$.

range of values of Pe'_p of interest in the present study are shown in Figure 1, where it is possible to observe the dependence of D_T on the Schmidt number for the range $Sc \leq 550$. An empirical correlation was found to describe the measured data of D_T for $Sc \leq 550$ (shown in Figure 1 as dashed lines)

$$\frac{D_T}{D'_m} = 1 + \frac{Pe'_p}{12} - \left(\frac{Sc}{1500}\right)^{4.8} Pe'^{4.83-1.3\log_{10}(Sc)}_p \qquad (11)$$

For $Sc > 550$ the transverse dispersion coefficient is found to be independent of the Schmidt number, and the correlation reduces to

$$\frac{D_T}{D'_m} = 1 + \frac{Pe'_p}{12} - 8.1 \times 10^{-3} Pe'^{1.268}_p \qquad (12)$$

As for D_L, it is fortunate that its value is not needed with accuracy, since for $Pe'_p > 1$, the boundary layer for mass transfer around the sphere is thin, provided that the approximate condition $d_1/d > 10$ is observed. Indeed, for $Pe'(= Pe'_p d_1/d) > 10$, the boundary layer is thin and the term with D_L in Eq. 5, can be neglected (Coelho and Guedes de Carvalho, 1988b); numerical computations were undertaken in the present work that confirm the insensitivity of Sh' to D_L, for $Pe' > 10$.

For each value of Sc indicated in Figure 1, Eq. 5 was solved numerically, with the point values of D_T given by the corresponding fitted curve (Eqs. 11 and 12). From the numerical simulations, plots of Sh'/ϵ vs. Pe' were prepared for given values of d/d_1 in a similar fashion to what was done by Guedes de Carvalho and Alves (1999); in the present case, a set of plots had to be made for each value of Sc. The results of the numerical computations are shown as points in Figure 2a–2d, and an expression was sought to describe the functional de-

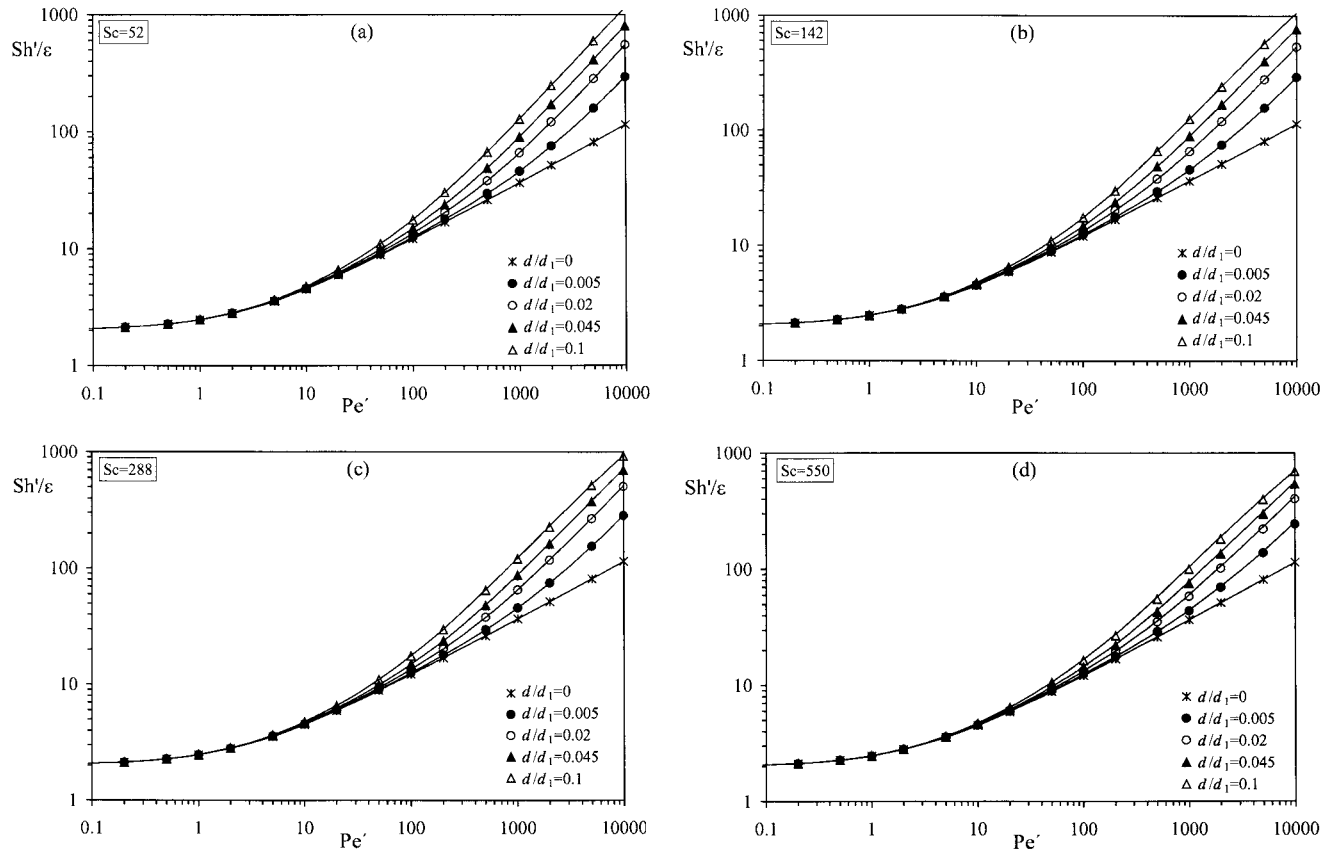

Figure 2. Dependence of $Sh'/å$ on Pe' for different values of d/d_1 at (a) $Sc = 52$; (b) $Sc = 142$; (c) $Sc = 288$; (d) $Sc = 550$: the points were obtained from the numerical solution of Eq. 5 and the solid lines represent Eq. 13.

pendence observed, with good accuracy. The following equation is proposed for $Sc \leq 550$

$$\frac{Sh'}{\epsilon} = \left[4 + \frac{4}{5}(Pe')^{2/3} + \frac{4}{\pi}Pe'\right]^{1/2} \times \left[1 + \frac{Pe'_p}{9} - \left(\frac{Sc}{1500}\right)^{4.8}\left(\frac{4}{3}Pe'_p\right)^{4.83-1.3\log_{10}(Sc)}\right]^{1/2} \quad (13)$$

For $Sc > 550$, the value of Sh' is independent of Sc, since D_T/D'_m is independent of Sc. Substituting $Sc = 550$ in Eq. 13 leads to

$$\frac{Sh'}{\epsilon} = \left[4 + \frac{4}{5}(Pe')^{2/3} + \frac{4}{\pi}Pe'\right]^{1/2} \times \left[1 + \frac{Pe'_p}{9} - 1.16 \times 10^{-2}Pe'^{1.268}_p\right]^{1/2} \quad (14)$$

and this can be expected to predict mass-transfer coefficients for $Sc \geq 550$. In the plots in Figure 2, the solid lines represent either Eq. 13 or Eq. 14, and it may be seen that they describe the results of the numerical computations with very good accuracy.

It is worth emphasizing some important features of Eqs. 13 and 14. First of all, the fact that the first term on the righthand side of both equations gives the dimensionless mass-transfer coefficient for low Pe'_p when both longitudinal and transverse dispersion are due to molecular diffusion alone ($D_L = D_T = D'_m$). This result was obtained by Guedes de Carvalho and Alves (1999), who emphasized the fact by writing (for $Pe'_p < 0.1$, say)

$$\frac{Sh'}{\epsilon} = \frac{Sh'_{md}}{\epsilon} = \left[4 + \frac{4}{5}(Pe')^{2/3} + \frac{4}{\pi}Pe'\right]^{1/2} \quad (15)$$

The second term (with square brackets) on the righthand side of Eqs. 13 and 14 is therefore the "enhancement factor" due to convective dispersion. It will be noticed that the enhancement factor is independent of Sc for high values of this parameter and dependent on Sc for $Sc \leq 550$. This is because mass-transfer rates around the sphere depend strongly on D_T and the value of D_T/D'_m is independent of Sc only for $Sc > 550$, as shown recently by Delgado and Guedes de Carvalho (2001) in a detailed study on dispersion in liquids.

A convenient way of presenting the result given by Eqs. 13 and 14 is then

$$\frac{Sh'}{\epsilon} = \frac{Sh'_{md}}{\epsilon} \cdot \eta, \quad (16)$$

with

$$\eta = \left[1 + \frac{Pe'_p}{9} - \left(\frac{Sc}{1500}\right)^{4.8}\left(\frac{4}{3}Pe'_p\right)^{4.83-1.3\log_{10}(Sc)}\right]^{1/2} \quad \text{for} \quad Sc \leq 550 \quad (17a)$$

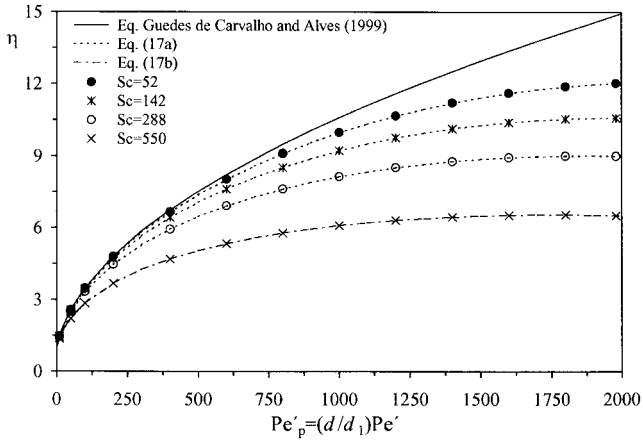

Figure 3. Dependence of η on Pe'_p for different values of Sc: the points were obtained from the numerical solution of Eq. 5.

and

$$\eta = \left[1 + \frac{Pe'_p}{9} - 1.16 \times 10^{-2}Pe'^{1.268}_p\right]^{1/2} \quad \text{for} \quad Sc > 550. \quad (17b)$$

It can be seen that η approaches unity as Pe'_p is reduced, and for gas flow, with $Sc \cong 1$, Eq. 17b is virtually coincident with $\eta = (1 + Pe'_p/9)^{1/2}$, which was the expression suggested by Guedes de Carvalho and Alves (1999). The values of η obtained from the numerical solution of Eq. 5 are represented as points in Figure 3, alongside the lines corresponding to Eqs. 17a,b. The scale is linear and it can be seen that the agreement is excellent.

Equations 16 and 17 therefore can be seen as a general result derived from first principles for mass transfer between a sphere of diameter d_1 buried in a packed bed of inerts of diameter d, and the fluid flowing through the interstices of the bed with velocity u_0 (at some distance from the sphere). Experiments were performed to test this result over a wide range of temperatures, as described in the next section.

Experiment

Experiments were performed on the dissolution of single-spheres of both benzoic acid and 2-naphthol, buried in beds of sand (0.219 mm or 0.496 mm average particle diameter) through which water was steadily forced down at temperatures in the range 293 K to 373 K.

Figure 4 shows the experimental rig (not to scale). The distilled water in the feed reservoir was initially dearated under vacuum to avoid freeing gas bubbles in the rig at high temperature. The test column was a stainless steel tube (100 mm ID and 500 mm long), and it was immersed in a silicone oil bath kept at the desired operating temperature by means of a thermosetting bath head (not represented in the figure). The copper tubing feeding the pressurized water to the column at a constant metered rate was partly immersed in a preheater, and it had a significant length immersed in the same thermosetting bath as the test column; the copper tubing leaving the test column was

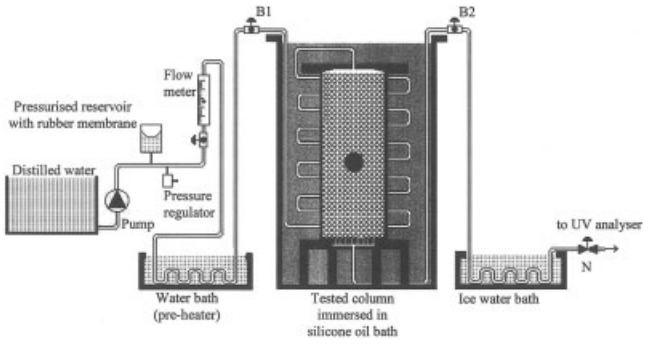

Figure 4. Experimental setup.

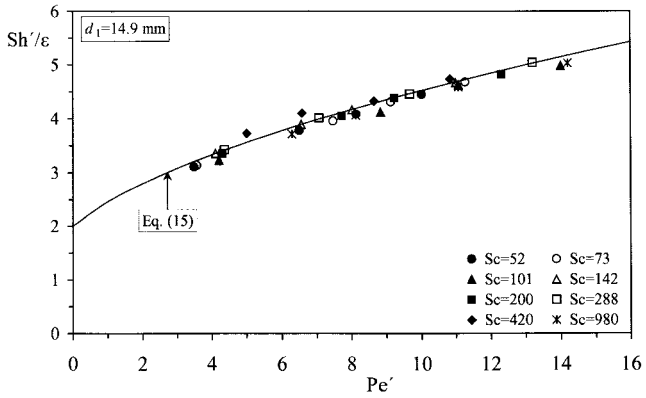

Figure 5. Dependence of Sh'/ϵ on Pe' for $D_T = D_L = D'_m$ (throughout).

immersed in a chiller to cool the outlet stream before reaching the UV analyzer.

In order to replace the sphere buried in the sand, valves B1 and B2 were closed, the lid of the test column was removed, and a source of distilled water was connected near N to direct water "backwards" to the test column. Valve B2 was then opened gently to reach incipient fluidization of the sand; the soluble sphere was then replaced, the water flow was immediately stopped, and the lid of the test column was placed back in position. The downflow of water through the test column was then initiated at a very low flow rate, while the column was immersed in the silicone oil bath and the temperature was allowed to rise (slowly) to the value intended for the experiment. The flow rate of water was then adjusted to the required value, v, and the concentration of solute in the outlet stream was continuously monitored by means of a UV/VIS Spectrophotometer (set at 274 nm for 2-naphthol, and at 226 nm for benzoic acid). The instant rate of dissolution of the sphere was calculated from the steady-state concentration of solute at the exit, c_e, as $n = vc_e$.

The spheres of benzoic acid and 2-naphthol were prepared from *p.a.* grade material, which was molten and then poured into moulds made of silicone rubber to give spheres with approximate diameters of 11, 15, 19, and 25 mm. If any slight imperfections showed on the surface of the spheres, they were easily removed by rubbing with fine sandpaper. Vernier callipers were used to make three measurements of the diameter of each sphere, along three perpendicular directions. The spheres would be discarded if the difference between any two measurements exceeded 1 mm; otherwise, they would be kept for the experiments and taken to have a diameter equal to the average of the three measurements.

The silica sand used in the experiments was previously washed, dried, and sieved in closely sized batches. Table 1 gives the corresponding size distribution, as determined by a laser diffraction technique.

Results and Discussion

Accurate values of c^* and D'_m are needed in the treatment of the mass-transfer data obtained in our experiments. Values of those parameters at different temperatures are given (and discussed) in Appendix B for the systems used.

In order to test Eq. 15, it was necessary to perform some experiments at very low Pe'_p. A significant number of data points were obtained with both benzoic acid and 2-naphthol and, in Figure 5, they are shown to be in excellent agreement with Eq. 15. The agreement is so good that in Appendix B we suggest that measuring the rate of dissolution of a buried sphere at low Pe'_p may be an accurate method for determining the molecular diffusion coefficient of slightly soluble solutes. At higher values of Pe'_p, it may be seen, from Eq. 13, that Sh'/ϵ is expected to be a function of d/d_1, Sc, and Pe', since $Pe'_p = Pe'(d/d_1)$.

Our experimental points were therefore organized in three plots of Sh'/ϵ vs. Pe' (one plot for each value of d/d_1), as shown in Figures 6, 7, and 8. These figures show that the agreement between experiment and Eqs. 13 and 14 is very good, and this is strong support for our theory.

In each of the plots of Figures 6–8, the solid line represents the equation for gas flow obtained and tested by Guedes de Carvalho and Alves (1999). It can be seen that the data obtained in the present work virtually bridge the gap between the extremes of gas flow ($Sc \cong 1$) and cold-water flow ($Sc = 980$). Also, the agreement between theory and experiment is excellent over the entire range; and since D_T/D_m is independent of Sc for $Sc \geq 550$ [see Delgado and Guedes de Carvalho (2001)], it can be stated that Eqs. 13 and 14 (or, alternatively, Eqs. 16 and 17a,b) accurately predict the coefficient of mass transfer between a sphere buried in a packed bed of inerts and the fluid flowing around it, in parallel uniform flow (far from

Table 1. Properties of the Sand Beds

Nominal Size (mm)	ϵ	τ	Particle Diameter ($< \mu$m) 10% vol.	20% vol.	30% vol.	40% vol.	50% vol.	60% vol.	70% vol.	80% vol.	90% vol.	100% vol.
0.219	0.40	1.41	161	180	195	210	225	241	259	281	313	476
0.496	0.34	1.41	277	340	389	434	480	530	588	660	756	900

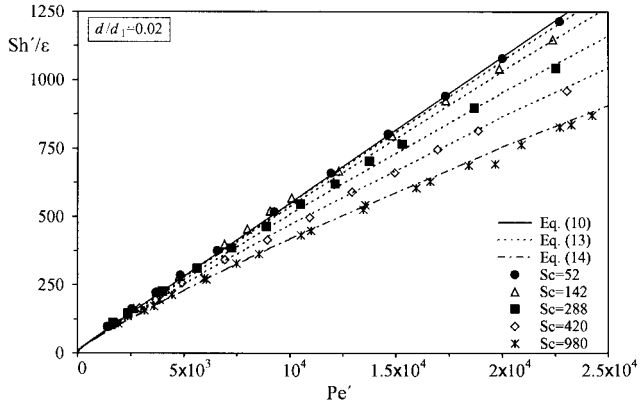

Figure 6. Comparison between experimental points (this work) for $d/d_1 = 0.02$ and the theory represented by Eqs. 13 and 14.

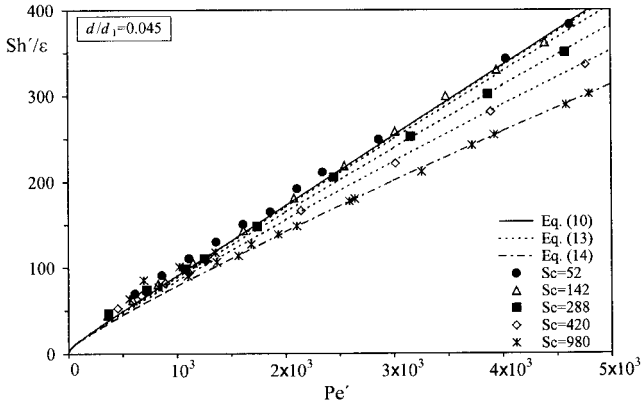

Figure 8. Comparison between experimental points (this work) for $d/d_1 = 0.045$ and the theory represented by Eqs. 13 and 14.

the sphere). The approximate conditions of validity of those equations are

$$Re_p < 25 \tag{18a}$$

$$d_1/d > 10 \tag{18b}$$

$$Pe'_p < 1300 \tag{18c}$$

and these are easily met in most situations of practical interest. The limitation on Re_p ensures that Darcy's law is observed with good approximation, $d_1/d > 10$ is an approximate condition establishing that the active particles are large compared to the inerts, and the limitation on Pe'_p is related to the dispersion data available (see Figure 1); it should be emphasized that near the surface of the sphere the fluid velocity varies up to $1.5u_0$.

Conclusions

The present work shows that a theory for mass transfer between a sphere buried in a packed bed of inerts and the fluid flowing past it may be derived from first principles, which is valid for any value of Sc. The numerical solution of the equation representing the theory gives the "exact" values of Sh'/ϵ, and these are well represented by Eqs. 13 and 14 (or, alternatively, by Eqs. 16 and 17a,b).

The large number of experimental points reported, covering a wide range of the relevant parameters, provide strong support for the theory developed.

In Figure 9 predictions of the theory presented in this work are compared with those given by equations proposed by other authors (see Table 2). Figure 9 refers only to one value of d/d_1 (similar curves are obtained for other values of d/d_1), and the two "extreme" values of $Sc = 1$ and $Sc = 980$, corresponding approximately to gas flow and cold water flow, respectively, are considered. With hot water (or other low-viscosity liquids) or supercritical fluids, the intermediate range of Sc is covered and the lines giving the different correlations are situated between the two extremes.

The large number of experimental values reported in the present work, together with the many available for gas flow [see Guedes de Carvalho and Alves (1999)], confirms the

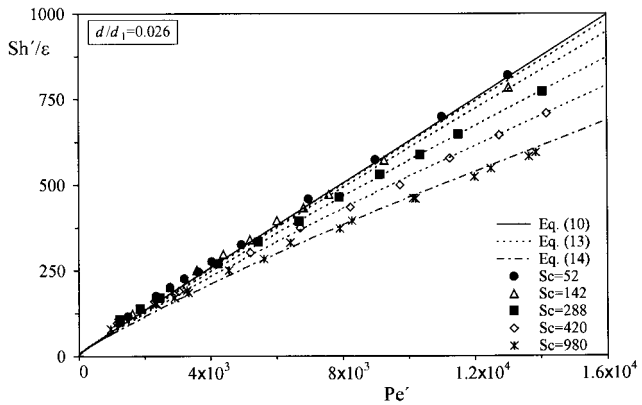

Figure 7. Comparison between experimental points (this work) for $d/d_1 = 0.026$ and the theory represented by Eqs. 13 and 14.

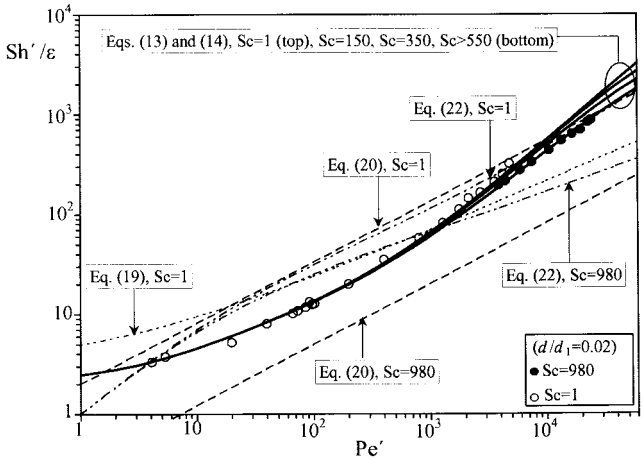

Figure 9. Comparison of equations available for the prediction of mass transfer from a buried sphere (the experimental points for $Sc = 1$ and $Sc = 980$ are a small sample of the available data).

Table 2. Equations Available in Literature for Mass Transfer from Large Active Particles in Beds of Small Inerts

Reference	Model	Equation
La Nauze et al. (1984)	$\frac{Sh'}{\epsilon} = 2\tau + \left(\frac{4\tau}{\pi\epsilon}\right)^{1/2}(Pe')^{1/2}$ (gas flow)	19
Prins et al. (1985)	$\frac{Sh'}{\epsilon} = K(Pe')^{1-m}$	20
	$K = \frac{\tau^m}{\epsilon}\left(\frac{1-\epsilon}{\epsilon}\right)^m\left(\frac{d_1}{d}\right)^m\left[0.105 + 1.505\left(\frac{d_1}{d}\right)^{-1.05}\right]Sc^{m-2/3}$	20a
	$m = 0.35 + 0.29\left(\frac{d}{d_1}\right)^{0.5}$	20b
Coelho and G. Carvalho (1988b)	$\frac{Sh'}{\epsilon} = \left[4 + 0.576(Pe')^{0.78} + 1.28(Pe') + 0.141\left(\frac{d}{d_1}\right)(Pe')^2\right]^{1/2}$	21
Agarwal et al. (1988)	$\frac{Sh'}{\epsilon} = K_p\frac{\tau}{\epsilon}\left(\frac{C_{D\epsilon a}}{8}\right)^{1/3}(Pe')^{1/3}Sc^{-1/3}$	22
	$K_p = 0.69\frac{[1 + (\epsilon/\tau)Pe']^{1/3} - 1}{[(\epsilon/\tau)Pe']^{1/3}}$	22a
	$C_{D\epsilon a} = \frac{24\tau^2 Sc}{\epsilon Pe'}\left[\frac{2Z(1-\epsilon)}{\tau} + 10^{\psi} - 1\right]$	22b
	$\psi = 0.261\left(\frac{\epsilon\cdot Pe'}{\tau\cdot Sc}\right)^{0.369} - 0.105\left(\frac{\epsilon\cdot Pe'}{\tau\cdot Sc}\right)^{0.431} - \frac{0.124}{1 + \left\{\mathrm{Log}\left(\frac{\epsilon\cdot Pe'}{\tau\cdot Sc}\right)\right\}^2}$	22c
	$Z = \frac{5.3}{\tau^2}\left(\frac{\epsilon}{1-\epsilon}\right)^{0.3}$	22d
G. Carvalho and Alves (1999)	$\frac{Sh'}{\epsilon} = \left[4 + \frac{4}{5}(Pe')^{2/3} + \frac{4}{\pi}Pe'\right]^{1/2}\left[1 + \frac{1}{9}\left(\frac{d}{d_1}\right)Pe'\right]^{1/2}$ (*gasflow*)	23

validity of Eqs. 13 and 14 over the entire range of Sc. A small sample of data points for naphthalene-air and 2-naphthol–water at ambient temperature are represented in Figure 9. It can be seen that the other equations give very inaccurate predictions over a wide range of values of Pe'_p.

Notation

A = area
c = solute concentration
c_0 = bulk concentration of solute
c^* = saturation concentration of solute
c_e = concentration in the outlet stream
C = dimensionless solute concentration (as defined in Eq. A1)
d = diameter of inert particles
d_1 = diameter of active sphere
D_L = longitudinal dispersion coefficient
D_m = molecular diffusion coefficient
D'_m = effective molecular diffusion coefficient ($= D_m/\tau$)
D_T = transverse (radial) dispersion coefficient
K = permeability in Darcy's law
k = average mass-transfer coefficient
n = mass-transfer rate
p = pressure
$Pe_L(\infty)$ = asymptotic value of Pe_L when $Re_p \to \infty$
$Pe_T(\infty)$ = asymptotic value of Pe_T when $Re_p \to \infty$
R = radius of the sphere
$\Re$ = dimensionless spherical radial coordinate ($= r/R$)
r = spherical radial coordinate (distance to the center of the soluble sphere)
U = dimensionless interstitial velocity ($= u/u_0$)
u = absolute value of interstitial velocity
$\boldsymbol{u}$ = interstitial velocity (vector)
u_0 = absolute value of interstitial velocity far from the active sphere
u_r, u_θ = components of fluid interstitial velocity
v = volumetric flow rate

Greek letters

ϵ = bed voidage
Φ = dimensionless potential function (as defined in Eq. A4)
ϕ = potential function (defined in Eq. 1)
η = enhancement factor due to convective dispersion (defined in Eq. 16)
μ = dynamic viscosity
θ = spherical angular coordinate
ρ = density
τ = tortuosity
ω = cyclindrical radial coordinate (distance to the axis)
Ψ = dimensionless stream function (as defined in Eq. A5)
ψ = stream function (defined in Eq. 2)

Dimensionless groups

Pe' = Peclet number based on diameter of active sphere ($= u_0 d_1/D'_m$)
Pe'_p = Peclet number based on diameter of inert particles ($= u_0 d/D'_m$)
Re_p = Reynolds number based on diameter of inert particles ($= \rho u d/\mu$)
Sc = Schmidt number ($= \mu/\rho D_m$)
Sh' = Sherwood number ($= k d_1/d'_m$)
Sh'_{md} = Sherwood number when $D_T = D_L = D'_m$ (i.e., $Pe'_p < 0.1$)

Subscripts and superscripts

i, j = grid node indices (see Figure A1)
n = iteration number

Literature Cited

Agarwal, P. K., W. J. Mitchell, and R. D. La Nauze, "Transport Phenomena in Multi-Particle Systems—III. Active Particle Mass Transfer in Fluidized Beds of Inert Particles," *Chem. Eng. Sci.,* **43,** 2511 (1988).

Coelho, M. N., and J. R. Guedes de Carvalho, "Transverse Dispersion in Granular Beds: Part I—Mass Transfer from a Wall and the Dispersion Coefficient in Packed Beds," *Chem. Eng. Res. Des.,* **66,** 165 (1988a).

Coelho, M. A. N., and J. R. F. Guedes de Carvalho, "Transverse Dispersion in Granular Beds: Part II—Mass Transfer from Large Spheres Immersed in Fixed or Fluidised Beds of Small Inert Particles," *Chem. Eng. Res. Des.,* **66,** 178 (1988b).

Currie, I. G., *Fundamental Mechanics of Fluids,* McGraw-Hill, New York, p. 150 (1993).

Delgado, J. M. P. Q., and J. R. F. Guedes de Carvalho, "Measurement of the Coefficient of Transverse Dispersion in Packed Beds Over a Range of Values of Schmidt Number (50–1000)," *Transport Porous Media,* **44**(1), 165 (2001).

Dunker, C., "Benzoic Acid," *Kirk-Othmer Encyclopedia of Chemical Technology,* Vol. 3, 2nd ed., Interscience, New York, p. 422 (1964).

Ferziger, J. H., and M. Peric, *Computational Methods for Fluid Dynamics,* Springer-Verlag, Berlin, p. 42 (1996).

Gaskell, P. H., and A. K. C. Lau, "Curvature Compensated Convective Transport: SMART, A New Boundedness Preserving Transport Algorithm," *Int. J. Numer. Methods Fluids,* **8,** 617 (1988).

Ghosh, U. K., S. Kumar, and S. N. Upadhyay, "Diffusion Coefficient in Aqueous Polymer Solutions," *J. Chem. Eng. Data,* **36,** 413 (1991).

Guedes de Carvalho, J. R. F., M. A. Alves, and J. M. P. Q. Delgado, "Determination of Molecular Diffusion Coefficient Through Measurement of Mass Transfer Around a Cylinder Exposed to Liquid Flow in a Packed Bed," *Int. J. Heat Technol.,* **19**(2), 95 (2001).

Guedes de Carvalho, J. R. F., and M. A. M. Alves, "Mass Transfer and Dispersion Around Active Sphere Buried in a Packed Bed," *AIChE J.,* **45,** 2495 (1999).

Guedes de Carvalho, J. R. F., and J. M. P. Q. Delgado, "Mass Transfer from a Large Sphere Buried in a Packed Bed Along Which Liquid Flows," *Chem. Eng. Sci.,* **50,** 1121 (1999).

Guedes de Carvalho, J. R. F., and J. M. P. Q. Delgado, "Lateral Dispersion in Liquid Flow Through Packed Beds at $Pe_m < 1400$," *AIChE J.,* **46**(5), 1089 (2000).

La Nauze, R. D., K. Jung, and J. Kastl, "Mass Transfer to Large Particles in Fluidised Beds of Smaller Particles," *Chem. Eng. Sci.,* **39,** 1623 (1984).

Lozar, J., C. Laguerie, and J. P. Couderc, "Diffusivité de l'Acide Benzoique dans l'Eau: Influence de la Température," *Can. J. Chem. Eng.,* **53,** 200 (1975).

McCune, L. K., and R. H. Wilhelm, "Mass and Momentum Transfer in Solid-Liquid System," *Ind. Eng. Chem.,* **41**(6), 1124 (1949).

Moyle, M. P., and M. Tyner, "Solubility and Diffusivity of 2-Naphthol in Water," *Ind. Eng. Chem.,* **45**(8), 1794 (1953).

Prins, W., T. P. Casteleijn, W. Draijer, and W. P. M. Van Swaaij, "Mass Transfer from a Freely Moving Single Sphere to the Dense Phase of a Gas Fluidised Bed of Inert Particles," *Chem. Eng. Sci.,* **40,** 481 (1985).

Sahay, H., S. Kumar, S. N. Upadhyay, and Y. Upadhyay, "Solubility of Benzoic Acid in Aqueous Polymeric Solutions," *J. Chem. Eng. Data,* **26,** 181 (1981).

Seidell, A., *Solubilities of Organic Compounds,* 3rd ed., Van Nostrand, New York (1941).

Steele, L. R., and C. J. Geankoplis, "Mass Transfer from a Solid Sphere to Water in Highly Turbulent Flow," *AIChE J.,* **5,** 178 (1959).

Vanadurongwan, V., C. Laguerie, and J. P. Couderc, "Diffusivité Moyenne de l'Acide Benzoique dans l'Eau Entre la Dilution Infinie et la Saturation—Influence de la Température," *Can. J. Chem. Eng.,* **54,** 460 (1976).

Wilhelm, R. H., "Progress Towards the a Priori Design of Chemical Reactors," *Pure Appl. Chem.,* **5,** 403 (1962).

Wilke, C. R., and P. Chang, "Correlation of Diffusion Coefficients in Dilute Solutions," *AIChE J.,* **1**(2), 264 (1955).

Appendix

In order to integrate Eq. 5 with auxiliary Eqs. 1 and 2, it is convenient to define the dimensionless variables

$$C = \frac{c - c_0}{c^* - c_0} \tag{A1}$$

$$U = \frac{u}{u_0} = \frac{(u_r^2 + u_\theta^2)^{1/2}}{u_0} \tag{A2}$$

$$\Re = \frac{r}{R} \tag{A3}$$

$$\Phi = \frac{4}{3}\frac{\phi}{u_0 d_1} \tag{A4}$$

$$\Psi = \frac{\psi}{u_0 d_1^2}. \tag{A5}$$

Equation 5 can be rearranged to

$$\frac{\partial C}{\partial \Phi} = \frac{\partial}{\partial \Phi}\left[A\frac{\partial C}{\partial \Phi}\right] + \frac{\partial}{\partial \Psi}\left[B\frac{\partial C}{\partial \Psi}\right], \tag{A6}$$

with

$$A = \frac{4}{3Pe'}\frac{D_L}{D'_m} \tag{A7}$$

$$B = \frac{3}{16}\frac{\Re^2 \sin^2\theta}{Pe'}\frac{D_T}{D'_m}, \tag{A8}$$

and the appropriate boundary conditions are

$$\Phi \rightarrow -\infty, \Psi \geq 0 \quad C \rightarrow 0 \tag{A9}$$

$$\Phi \rightarrow +\infty, \Psi \geq 0 \quad C \rightarrow 0 \tag{A10}$$

$$\Psi = 0 \begin{cases} -1 \leq \Phi \leq 1 & C = 1 \quad \text{(A11a)} \\ |\Phi| > 1 & \dfrac{\partial C}{\partial \Psi} = 0 \quad \text{(A11b)} \end{cases}$$

$$\Psi \rightarrow +\infty, \quad \text{all} \quad \Phi \quad C \rightarrow 0 \tag{A12}$$

Discretization

Equation A6 was solved numerically using a finite difference method similar to that adopted by Guedes de Carvalho and Alves (1999). A second-order central differencing scheme (CDS) in a general nonuniform grid was adopted for the discretization of the diffusive terms (Ferziger and Peric, 1996) that appear on the righthand side of Eq. A6. The convection term that appears on the lefthand side of Eq. A6 was discretized with the SMART high-resolution scheme of Gaskell and Lau (1988), which preserves boundedness even for convective dominated flows.

The discretized equation resulting from the finite difference approximation of Eq. A6 reads

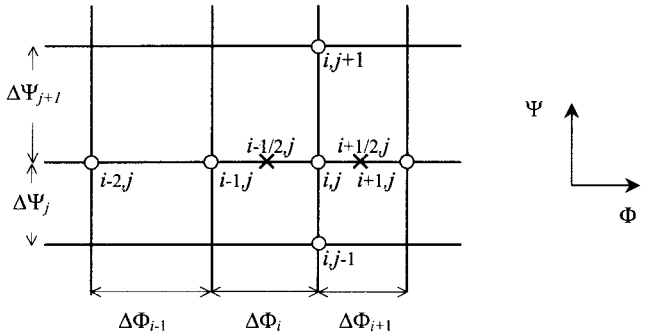

Figure A1. Computational grid.

$$\frac{C_{i+1/2,j}-C_{i-1/2,j}}{\Phi_{i+1/2}-\Phi_{i-1/2}}=\frac{A_{i+1/2}\dfrac{C_{i+1,j}-C_{i,j}}{\Phi_{i+1}-\Phi_i}-A_{i-1/2}\dfrac{C_{i,j}-C_{i-1,j}}{\Phi_i-\Phi_{i-1}}}{\Phi_{i+1/2}-\Phi_{i-1/2}}+\frac{B_{j+1/2}\dfrac{C_{i,j+1}-C_{i,j}}{\Psi_{j+1}-\Psi_j}-B_{j-1/2}\dfrac{C_{i,j}-C_{i,j-1}}{\Psi_j-\Psi_{j-1}}}{\Psi_{j+1/2}-\Psi_{j-1/2}},\quad\text{(A13)}$$

where the values of the Φ, Ψ, A, and B coefficients are easily computed using their definitions (Eqs. A4, A5, A7, and A8). Please note that these coefficients only have to be computed once, since they are dependent on *a priori* known quantities, and are not influenced by the unknown concentration field.

The $C_{i+1/2,j}$ and $C_{i-1/2,j}$ values have to be conveniently interpolated from the known grid node values (represented as circles in Figure A1) using the SMART high-resolution scheme to ensure numerical stability and good precision:

$$C_{i+1/2,j}=C_{i-1,j}+\hat{C}_{i+1/2,j}(C_{i+1,j}-C_{i-1,j}).\quad\text{(A14)}$$

The limiter function $\hat{C}_{i+1/2,j}$ used in this work is expressed as (Gaskell and Lau, 1988)

$$\hat{C}_{i+1/2,j}=\begin{cases}3\dfrac{C_{i,j}-C_{i-1,j}}{C_{i+1,j}-C_{i-1,j}} & \text{if}\quad \dfrac{C_{i,j}-C_{i-1,j}}{C_{i+1,j}-C_{i-1,j}}\in\left[0,\dfrac{1}{6}\right[\\ \dfrac{3}{8}+\dfrac{3}{4}\dfrac{C_{i,j}-C_{i-1,j}}{C_{i+1,j}-C_{i-1,j}} & \text{if}\quad \dfrac{C_{i,j}-C_{i-1,j}}{C_{i+1,j}-C_{i-1,j}}\in\left[\dfrac{1}{6},\dfrac{5}{6}\right]\\ 1 & \text{if}\quad \dfrac{C_{i,j}-C_{i-1,j}}{C_{i+1,j}-C_{i-1,j}}\in\left]\dfrac{5}{6},1\right]\\ \dfrac{C_{i,j}-C_{i-1,j}}{C_{i+1,j}-C_{i-1,j}} & \text{if}\quad \dfrac{C_{i,j}-C_{i-1,j}}{C_{i+1,j}-C_{i-1,j}}\notin[0,1],\end{cases}\quad\text{(A15)}$$

or, in compact form

$$\hat{C}_{i+1/2,j}=\max\left[\frac{C_{i,j}-C_{i-1,j}}{C_{i+1,j}-C_{i-1,j}},\min\left(3\frac{C_{i,j}-C_{i-1,j}}{C_{i+1,j}-C_{i-1,j}},\frac{3}{4}+\frac{3}{8}\frac{C_{i,j}-C_{i-1,j}}{C_{i+1,j}-C_{i-1,j}},1\right)\right]\quad\text{(A16)}$$

Similarly, for the left face relative to node (i, j), one obtains

$$C_{i-1/2,j}=C_{i-2,j}+\hat{C}_{i-1/2,j}(C_{i,j}-C_{i-2,j}),\quad\text{(A17)}$$

with

$$\hat{C}_{i-1/2,j}=\max\left[\frac{C_{i-1,j}-C_{i-2,j}}{C_{i,j}-C_{i-2,j}},\min\left(3\frac{C_{i-1,j}-C_{i-2,j}}{C_{i,j}-C_{i-2,j}},\frac{3}{8}+\frac{3}{4}\frac{C_{i-1,j}-C_{i-2,j}}{C_{i,j}-C_{i-2,j}},1\right)\right]\quad\text{(A18)}$$

Substitution of Eqs. A14 and A17 into Eq. A13 leads to the final form of the discretized equation, which can be cast in compact form as

$$C_{i,j}=(FC_{i-2,j}+GC_{i-1,j}+HC_{i+1,j}+IC_{i,j-1}+JC_{i,j+1})/E.\quad\text{(A19)}$$

The resulting system of equations (Eq. A19) was solved iteratively using the successive overrelaxation (SOR) method (Ferziger and Peric, 1996), and the implementation of the boundary conditions was done in the same way as described in our previous work (Guedes de Carvalho and Alves, 1999).

It should be noted that we always started our calculations with a zero concentration field on a coarse grid. A converged solution could be obtained very quickly (O(10 s) in a desktop PC with a 1.4 GHz AMD processor), and then we proceeded to a finer grid (doubling the number of grid points in each direction). Instead of restarting the calculations with a zero concentration field in this new finer grid, we simply interpolated the solution obtained in the coarse-level grid, leading to a significant decrease in the CPU time required to attain convergence. This fully automated procedure was repeated until the finest mesh calculations were performed. The use of Richardson's extrapolation to the limit allowed us to obtain very accurate solutions (with errors in the computed Sh' value below 0.1%). A more elaborate multigrid technique could have been implemented to further increase the convergence rate, but we found that this simple technique was sufficient to obtain mesh-independent solutions in affordable CPU times.

The converged solution obtained yields values of $C_{i,j}$, from which the overall mass-transfer rate from the sphere, n, could be calculated and expressed by means of an average Sherwood number

$$Sh'=\frac{kd_1}{D'_m}=[n/(\pi d_1^2)(c^*-c_0)]d_1/D'_m.\quad\text{(A20)}$$

The value of n was evaluated by numerically integrating the diffusive/dispersive flux of solute perpendicular to the sphere along its surface (Eq. 6)

$$n=-\epsilon\sum_i D_T R\sin(\theta_i)\frac{3}{2}u_0\sin(\theta_i)\times\left(\frac{\partial c}{\partial\psi}\right)_{i,1}2\pi R^2\left[\frac{\cos(\theta_{i-1})-\cos(\theta_{i+1})}{2}\right],\quad\text{(A21)}$$

which in dimensionless discretized form reads

$$\frac{Sh'}{\epsilon}=-\frac{3}{8}\sum_i\left(\frac{D_T}{D'_m}\right)_{i,1}\sin^2(\theta_i)\times\left(\frac{\partial C}{\partial\Psi}\right)_{i,1}\left[\frac{\cos(\theta_{i-1})-\cos(\theta_{i+1})}{2}\right].\quad\text{(A22)}$$

Appendix B: Relevant Properties of the 2-Naphthol–Water and Benzoic Acid–Water Systems

In the interpretation and correlation of the experimental data reported, it is important to know the solubility and the coefficient of molecular diffusion of 2-naphthol in water and of benzoic acid in water, in the range 293 K to 373 K.

Data from a number of sources are plotted in Figures B1 to B2 for the 2-naphthol–water system. The majority of data points are from McCune and Wilhelm (1949) and Moyle and Tyner (1953); the latter also provide the fitted functions

$$c^* = 5.93 \times 10^{-6}\exp(0.0394T) \quad \text{(B1)}$$

and

$$D_m = 9.95 \times 10^{-7}\exp(-2012/T), \quad \text{(B2)}$$

and these are drawn in the figures (c^* in kg/m^3, D_m in m^2/s, and T in K).

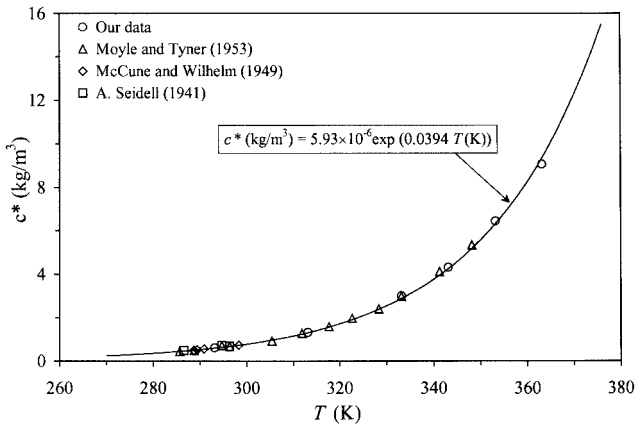

Figure B1. Solubility of 2-naphthol in water.

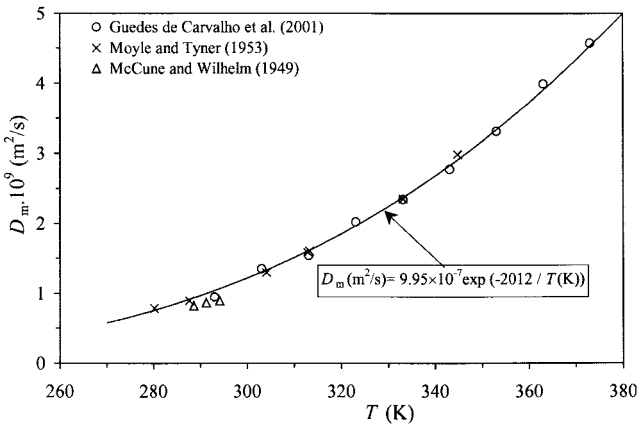

Figure B2. Coefficient of molecular diffusion for 2-naphthol in water.

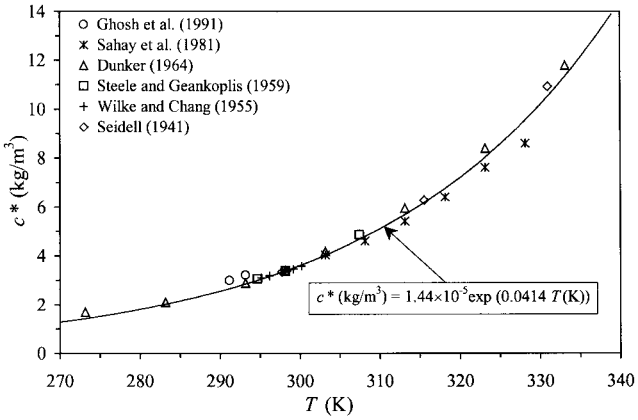

Figure B3. Solubility of benzoic acid in water.

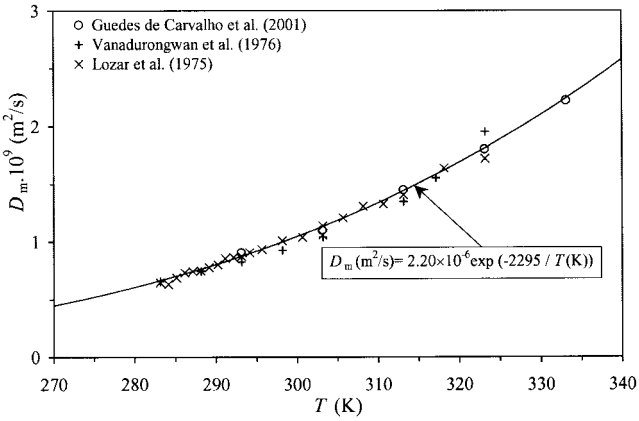

Figure B4. Coefficient of molecular diffusion for benzoic acid in water.

We performed some measurements of c^*, by saturating water with 2-naphthol up to 363 K, and obtained the points in Figure B1, in excellent agreement with the line proposed by Moyle and Tyner (1953). From our measurements of the mass-transfer rate around buried spheres at very low Pe'_p, values of D_m were also obtained, making use of Eq. 10. The corresponding points are also shown in Figure B2, and they clearly confirm the validity of Eq. B2.

For the benzoic acid–water system, a very large number of data points are available in the literature, as shown in Figures B3 and B4. The lines on those figures are given by the equations

$$c^* = 1.44 \times 10^{-5}\exp(0.0414T) \quad \text{(B3)}$$

and

$$D_m = 2.20 \times 10^{-6}\exp(-2295/T) \quad \text{(B4)}$$

that were fitted to the data points shown.

Manuscript received Apr. 10, 2002, revision received May 24, 2003, and final version received Aug. 11, 2003.